Title

Phosphatidylinositol-(4, 5)-bisphosphate regulates calcium gating of small-conductance cation channel TMEM16F.

Journal

Proceedings of the National Academy of Sciences of USA, 115(7)

Authors

Ye, Wenlei
Han, Tina
Nassar, Layla
et al.

Publication Date

2018-02-13

DOI

10.1073/pnas.1718728115

Peer reviewed

Phosphatidylinositol-(4, 5)-bisphosphate regulates calcium gating of small-conductance cation channel TMEM16F

Wenlei Ye[a], Tina W. Han[a], Layla M. Nassar[b], Mario Zubia[a], Yuh Nung Jan[a,b,c], and Lily Yeh Jan[a,b,c,1]

[a]Department of Physiology, University of California, San Francisco, CA 94158; [b]Howard Hughes Medical Institute, University of California, San Francisco, CA 94158; and [c]Department of Biochemistry and Biophysics, University of California, San Francisco, CA 94158

Contributed by Lily Yeh Jan, January 4, 2018 (sent for review October 26, 2017; reviewed by Bertil Hille and Paul A. Slesinger)

TMEM16F, which is activated by elevation of intracellular calcium to trigger phospholipid scrambling and the collapse of lipid bilayer asymmetry to mediate important cellular functions such as blood coagulation, also generates a small-conductance calcium-activated cation current. How TMEM16F activation may be regulated is an open question. By recording TMEM16F Ca^{2+}-activated current, we found that the TMEM16F Ca^{2+}-response is desensitized by a brief exposure to high intracellular Ca^{2+}, which is associated with depletion of phosphatidylinositol-(4, 5)-bisphosphate (PIP_2) from the inner leaflet of the membrane. Application of artificial or natural PIP_2 restores TMEM16F channel activity. PIP_2 modulation of TMEM16F requires the presence of several positively charged amino acids in its cytoplasmic N-terminal domain. TMEM16F interaction with PIP_2 works synergistically with membrane depolarization to facilitate Ca^{2+}-gating of TMEM16F. Our study reveals the dependence of TMEM16F activity on phosphoinositides and provides one mechanism for TMEM16F activation to be strictly regulated in the cell membrane.

TMEM16F | scramblase | phosphoinositide | PIP_2

The asymmetric distribution of phospholipids in the two leaflets of cellular membrane is evolutionarily conserved and critical for physiology (1). Phosphatidylserine, phosphatidylethanolamine, and phosphatidylinositol (PI) are present predominantly in the inner leaflet (on the cytosolic side) of the lipid bilayer (1). Disruption of lipid bilayer asymmetry via phospholipid scrambling initiates biological processes such as blood coagulation and cell apoptosis (2–4). Recent studies have shown that TMEM16F is required for the Ca^{2+}-activated phospholipid scrambling that is crucial for blood coagulation (5–7). TMEM16F is also the pore-forming subunit of a small-conductance Ca^{2+}-activated cation channel that permeates Ca^{2+} (6). TMEM16F-mediated Ca^{2+}-influx may serve as positive feedback to facilitate phospholipid scrambling (8). It is therefore important to regulate TMEM16F activity so as to prevent Ca^{2+}-overloading and cytotoxicity. In this study, we test whether elevated intracellular Ca^{2+} and some components of membrane lipids can regulate TMEM16F activity.

TMEM16F belongs to a transmembrane protein family (TMEM16) with diverse functions (8–10). Of the 10 members of the mammalian TMEM16 family, TMEM16A and TMEM16B form Ca^{2+}-activated chloride channels (11–13), while TMEM16F and some of its close relatives are required for phospholipid scrambling (5, 14). TMEM16 family members are all predicted to have 10 transmembrane helices (TM1–10) with N-terminal and C-terminal cytoplasmic domains (15, 16). TM3–TM8 form a hydrophilic pore or groove for the passage of ions or hydrophilic headgroups of phospholipids (15, 16). The current mediated by TMEM16F coincides with the scramblase activity, and therefore it has been proposed that this current corresponds to the ionic leak associated with the membrane phospholipid translocation (17, 18). Thus, the TMEM16F current precisely probed with electrophysiological techniques may reflect the extent of phospholipid scrambling, which is not readily quantifiable. As TMEM16F is a Ca^{2+}-permeable ion channel (6), TMEM16F current modulation may influence the Ca^{2+}-dependent phospholipid scrambling. We therefore propose to study TMEM16F from an ion-channel perspective.

Phosphoinositides are minor but functionally significant constituents of cellular membranes (19). The inositol ring of PI can be phosphorylated at multiple positions in numerous combinations to generate diverse phosphoinositides, many of which are present in mammalian cells and are differentially distributed in organellar membranes (1, 19). Phosphatidylinositol-(4, 5)-bisphosphate (PIP_2), one of the most abundant phosphoinositides, is mainly localized to the inner leaflet of cellular membranes. PIP_2 regulates many ion channels such as Kir, KCNQ, and TRP channels (20–25). Depending on the affinity of channel–PIP_2 interaction, PIP_2 functions either as permissive ligands that enable channels to open and conduct ions or as signaling molecules that regulate ion-channel activities (20, 21, 25). Given that PIP_2 is restricted to the plasma membrane and absent from other organellar membranes, a dependence of TMEM16F activity on PIP_2 could limit the Ca^{2+}-evoked activities of TMEM16F to the cell membrane (23, 25). The dynamic distribution of PIP_2 may allow it to act as a signaling molecule to facilitate or terminate TMEM16F activities. For these reasons, we set forth to test the hypothesis that TMEM16F function is dependent on PIP_2.

Significance

TMEM16F, a small-conductance Ca^{2+}-activated cation channel that permeates Ca^{2+}, is required for the Ca^{2+}-activated phospholipid scramblase activity. The Ca^{2+}-activated Ca^{2+}-conductance mediated by TMEM16F constitutes positive feedback, with potentially deleterious outcomes if not tightly regulated. We performed electrophysiological recordings to show that Ca^{2+}-gating of TMEM16F depends on TMEM16F interaction with PIP_2, a minor yet functionally significant phospholipid constituent in the plasma membrane. Elevated intracellular Ca^{2+} promotes PIP_2 hydrolysis by membrane-tethered phospholipases, thereby causing TMEM16F inactivation and likely rendering protection from Ca^{2+}-overloading and cytotoxicity. Given that TMEM16F plays significant roles in blood coagulation and immune responses, our study will help reveal how signaling pathways involving phosphoinositides could potentially contribute to these physiological processes.

Author contributions: W.Y., T.W.H., and L.Y.J. designed research; W.Y., T.W.H., and L.M.N. performed research; W.Y., T.W.H., and M.Z. contributed new reagents/analytic tools; W.Y., L.M.N., and L.Y.J. analyzed data; and W.Y., T.W.H., M.Z., Y.N.J., and L.Y.J. wrote the paper.

Reviewers: B.H., University of Washington School of Medicine; and P.A.S., Icahn School of Medicine at Mount Sinai.

The authors declare no conflict of interest.

[1]To whom correspondence should be addressed. Email: Lily.Jan@ucsf.edu.

This article contains supporting information online at www.pnas.org/lookup/suppl/doi:10.1073/pnas.1718728115/-/DCSupplemental.

In this study, we demonstrate PIP_2 regulation of TMEM16F. Depletion of PIP_2 caused by elevated cytoplasmic Ca^{2+} or PIP_2 scavengers elicits TMEM16F current rundown and desensitization to Ca^{2+}, which can be reversed by addition of exogenous PIP_2 or Mg-ATP for PIP_2 resynthesis. We identify a cluster of basic amino acids in the N-terminal domain that are essential for the modulation of TMEM16F by PIP_2 and reveal a synergy between membrane depolarization and TMEM16F interaction with PIP_2 in regulating Ca^{2+}-gating of TMEM16F. We thus conclude that TMEM16F function is dependent on its interaction with PIP_2.

Results

Elevated Intracellular Ca^{2+} Triggers Rundown and Desensitization of TMEM16F Current. In addition to its involvement in Ca^{2+}-activated phospholipid scrambling, TMEM16F functions as a small-conductance Ca^{2+}-activated ion channel, which allows us to study its activation kinetics by measuring the Ca^{2+}-activated current with recording from inside-out patches (6, 17). NaCl-based solutions with various concentrations of Ca^{2+} were perfused to the cytosolic side of the membrane excised from *Tmem16f-mcherry*–transfected human embryonic kidney (HEK293) cells. Because TMEM16F current is strongly outwardly rectifying, we recorded the outward current by holding the membrane potential at +80 mV for accurate measurement. An outward current was activated upon the application of Ca^{2+}, and the current magnitude was dose-dependent (Fig. 1*A*). Current rundown was observed with the application of 100 μM Ca^{2+}. The rundown was much faster in 1 mM Ca^{2+} (Fig. 1*A*), leading to a drastic reduction of the current magnitude and rapid inactivation. It thus appears that the rundown induced by exposure to 1 mM Ca^{2+} masked the full activation. Repeated applications of low levels of Ca^{2+} (≤19 μM) did not cause any decrease in current magnitude, whereas perfusion with high Ca^{2+} (≥100 μM) triggered current rundown in just a few seconds (Fig. S1*A*). For consistent measurement of the extent of current rundown, we exposed the excised membrane patch to 1 mM Ca^{2+} for about 60 s until the current decay reached a plateau, corresponding to a reduction by 53 ± 5% (Fig. 1*B*).

Further scrutiny of this current rundown revealed that the Ca^{2+} sensitivity of the channel was reduced along with the current magnitude. The current reached nearly maximal activation in the presence of 19 μM Ca^{2+} before exposure to high levels of Ca^{2+}, but the extent of current activation at various Ca^{2+} concentrations was greatly reduced after rundown was induced by the application of 1 mM Ca^{2+}, thus revealing desensitization of the Ca^{2+}-response (Fig. 1 *A* and *B* and Fig. S1*A*). We compared the Ca^{2+} sensitivity before and after prolonged exposure to 1 mM Ca^{2+} (~60 s). Normalized Ca^{2+}-elicited current magnitudes before and after desensitization exhibited a significant shift of the EC_{50} from 7.0 ± 0.8 μM to 45 ± 5 μM [Hill coefficient (H) = 2.1 ± 0.1 and 2.5 ± 0.3, respectively] (Fig. 1*C*). We then

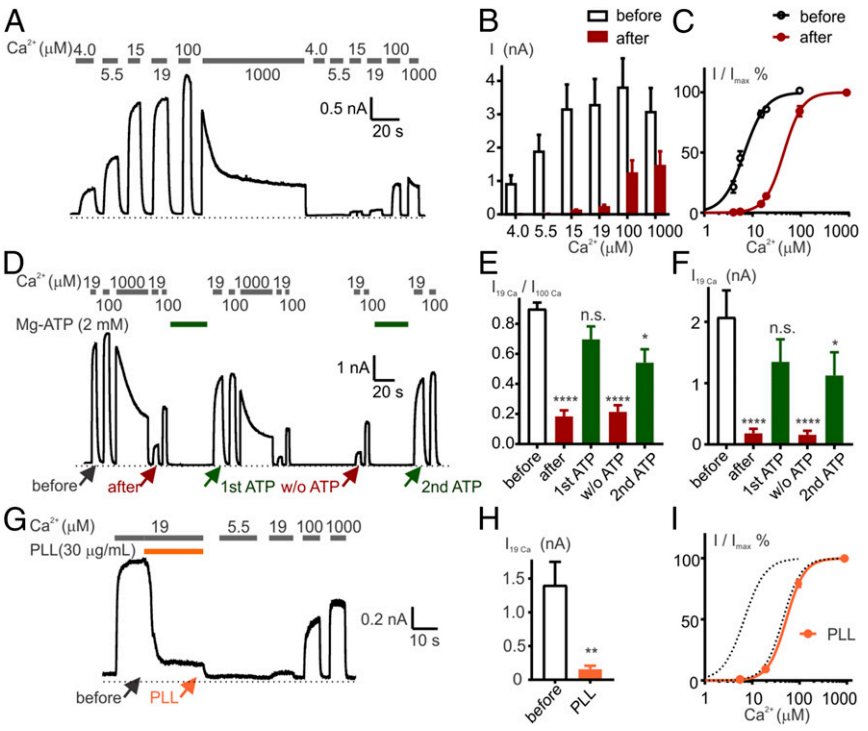

Fig. 1. PIP_2 depletion underlies TMEM16F current rundown and desensitization. (*A*) Representative recording of an inside-out patch (held at +80 mV) from a *Tmem16f-mcherry*–transfected cell. (*B*) Summary of current magnitudes (peak magnitudes for currents with decay) in the presence of various concentrations of Ca^{2+} as indicated, before and after exposure to 1 mM Ca^{2+} for ~60 s. $P < 0.01$ between the two groups (two-way ANOVA); $n = 6$. (*C*) Ca^{2+} sensitivity of TMEM16F current before and after exposure to 1 mM Ca^{2+}. The normalized current amplitudes were fit with the Hill equation. $P < 0.05$ in the difference of EC_{50} between the two groups (Wilcoxon matched-pairs test); $n = 6$. (*D*) Representative recording showing restoration from TMEM16F desensitization following the application of 2 mM Mg-ATP. Pairs of perfusion with 19 μM Ca^{2+} and 100 μM Ca^{2+} were applied repeatedly to estimate the extent of desensitization. (*E*) Summary of the current magnitudes in 19 μM Ca^{2+} normalized by currents in 100 μM Ca^{2+} ($I_{19\ Ca}/I_{100\ Ca}$) for each pair of perfusions in succession, at time points indicated by arrows. (*F*) Summary of current magnitudes in 19 μM Ca^{2+} at time points indicated by arrows. All values in *E* and *F* were compared with those before desensitization using one-way ANOVA followed by corrected Tukey post hoc tests. ****$P < 0.0001$, *$P < 0.05$, n.s. $P > 0.05$; $n = 9$. (*G*) Representative recording showing TMEM16F desensitization triggered by the application of 30 μg/mL PLL. (*H*) Comparison of current magnitudes at time points indicated by arrows. **$P < 0.01$ (paired *t* test) $n = 6$. (*I*) Ca^{2+} sensitivity after the treatment with PLL. Dotted lines are replotted from *C*. The Kruskal–Wallis test suggested there were significant differences in EC_{50} among the three groups, and the subsequent Dunn's multiple comparison test suggested the EC_{50} of the PLL-treated group was significantly different from control recorded before exposure to 1 mM Ca^{2+} ($P < 0.01$) but not from control recorded after exposure to 1 mM Ca^{2+} ($P = 0.6$).

tested whether the TMEM16F current was desensitized at physiological Ca^{2+} concentrations. Among all the tested conditions, 36 μM was the lowest concentration of Ca^{2+} that elicited significant current decay within ∼20 s (Fig. S2*A*), while 19 μM was the highest concentration of Ca^{2+} that did not. The Ca^{2+} sensitivity of TMEM16F was significantly reduced after ∼3 min of exposure to 36 μM Ca^{2+}, compared with the untreated group (Fig. S2*C*), and the current decay time was increased and became more variable (Fig. S2*B*). Whereas it is possible that lower Ca^{2+} could cause TMEM16F desensitization to develop over time, in the following experiments we used 1 mM Ca^{2+} to trigger desensitization to obtain recording results with minimal variability.

PIP_2 Depletion Underlies the Rundown and Desensitization of TMEM16F Current. Because we held the membrane potential at +80 mV for inside-out patch recordings of TMEM16F channels that permeate cations, we wondered whether current desensitization could be accounted for by accumulation of Ca^{2+} on the extracellular side of the membrane. We compared the Ca^{2+}-response curves recorded with either 0 mM Ca^{2+} (chelated with EGTA) or 5 mM Ca^{2+} in the pipette solution and found no significant difference, suggesting that desensitization is not influenced by accumulation of outwardly flowing Ca^{2+} ions on the extracellular side (Fig. S1*B*).

High cytosolic calcium causes depletion of PIP_2 through various mechanisms, such as promoting the activation of membrane-tethered phospholipases (26, 27). If TMEM16F desensitization is caused by depletion of PIP_2, it should be possible to reverse this desensitization by applying Mg-ATP, which allows PIP_2 to be generated via PI phosphorylation by membrane-tethered kinases (20). Indeed, 30-s perfusion of 2 mM Mg-ATP to the intracellular side of membrane significantly increased the current magnitude compared with current recorded from the same membrane patch but without the Mg-ATP treatment (Fig. 1 *D* and *F*). The recovery was not complete, possibly due to the exhaustion of PI in the patch and/or irreversible channel rundown from unknown mechanisms. As shown for the Ca^{2+}-response curves in Fig. 1*C*, the current in 19 μM Ca^{2+} normalized to the current in 100 μM Ca^{2+} ($I_{19\ Ca}/I_{100\ Ca}$) provides a rough estimate of the extent of desensitization: the smaller this ratio, the greater the desensitization. Treatment with Mg-ATP restored the Ca^{2+} sensitivity as well as the current magnitude reproducibly, with $I_{19\ Ca}/I_{100\ Ca}$ being 0.70 ± 0.09 ("1st ATP") and 0.54 ± 0.09 ("2nd ATP"), comparable to 0.90 ± 0.04 at the beginning of the recording ("before" condition). In contrast, without the Mg-ATP treatment, the current desensitization was persistent ($I_{19\ Ca}/I_{100\ Ca}$ = 0.21 ± 0.04, "w/o ATP" condition) and did not recover after the exposure to 1 mM Ca^{2+} (0.18 ± 0.04) ("after" condition) (Fig. 1*E*). Moreover, application of 30 μg/mL poly-L-lysine (PLL), a PIP_2 scavenger, caused current rundown in 19 μM Ca^{2+}, a condition where TMEM16F normally showed no desensitization (Fig. 1 *G* and *H*). The Ca^{2+} sensitivity after PLL treatment mimicked that of channels exposed to 1 mM Ca^{2+} (Fig. 1*I*). It thus appears that elevation of intracellular Ca^{2+} caused TMEM16F rundown and desensitization via depletion of PIP_2. These results suggest that TMEM16F functions are dependent on PIP_2.

Exogenous Application of PIP_2 Rescues TMEM16F from Desensitization. To test the hypothesis that depletion of PIP_2 underlies TMEM16F desensitization, we applied dipalmitoyl-PIP_2 (di-C_{16} PIP_2) to the desensitized channels and found that this treatment led to recovery of the current. Repeated applications of di-C_{16} PIP_2 revealed that the occurrence of current restoration correlated with the presence of PIP_2 (Fig. 2*A*). During the two applications of di-C_{16} PIP_2 (dissolved in solution containing 19 μM Ca^{2+}), the current magnitude increased by 2.48 ± 0.18- and 1.69 ± 0.25-fold, respectively. In contrast, exposure to 19 μM Ca^{2+} alone did not significantly change the current magnitude (1.09 ± 0.08- and 1.03 ± 0.04-fold, respectively) (Fig. 2*B*). We also calculated $I_{19\ Ca}/I_{100\ Ca}$ to assess the extent of desensitization. Accompanying the current recovery was the restoration of TMEM16F Ca^{2+} sensitivity (Fig. 2*C*).

We then tested if natural PIP_2 could also rescue TMEM16F current from desensitization. The PIP_2 purified from swine brains has 1-stearoyl-2-arachidonoyl-sn-glycero-3-phosphoinositol-4,5-bisphosphate [18:0–20:4-PI(4,5)P_2] as its major component. Application of 20 μM natural PIP_2 led to restoration of TMEM16F current from desensitization; the current amplitude continued to increase after wash-off of PIP_2 (Fig. 2*D*), likely due to the lateral movement of PIP_2 that had been incorporated in the excised membrane. Normalized against the current magnitude activated by 100 μM Ca^{2+}, the currents elicited by 19 μM Ca^{2+} dropped from the nearly maximally activated current magnitude before exposure to 1 mM Ca^{2+} ("before" condition) to 0.04 ± 0.01 ("desensitized"), then gradually increased to 0.16 ± 0.09 during PIP_2 application ("+ PIP_2") and 0.38 ± 0.13 after wash-off of PIP_2 ("wash PIP_2") (Fig. 2*E*). In contrast, recovery from TMEM16F desensitization was minor without PIP_2 application when assessed at time points ("pre" and "post") comparable to those examined in recordings with PIP_2 application (Fig. 2*F*). Two-way ANOVA analysis with Sidak's multiple-comparison test suggested that there was a significant difference between control and the PIP_2-treated group (Fig. 2*G*).

di-C_8 PIP_2 Interaction with TMEM16F Was Reversible. We noticed that the restoration of TMEM16F current by di-C_{16} PIP_2 and natural PIP_2 persisted even after wash-off. Both di-C_{16} PIP_2 and natural PIP_2 have acyl chains similar in length to those of membrane phospholipids, so they could be stably incorporated into the membrane. To ask whether the irreversible current restoration could be explained by the stable incorporation of PIP_2 into membrane or the irreversible binding of PIP_2 to TMEM16F, we used di-C_8 PIP_2, which could be quickly removed from the membrane due to its short acyl chains. The current restoration by di-C_8 PIP_2 was more rapid in its onset, but the effect did not persist upon removal of di-C_8 PIP_2 (Fig. 3 *A* and *B*). This suggests that the interaction between PIP_2 and TMEM16F is reversible and that the irreversible restoration of channel activity by di-C_{16} PIP_2 or natural PIP_2 is due to the ability of PIP_2 with long acyl chains to remain associated with the membrane.

Taking advantage of the reversible restoration of TMEM16F channel activity by di-C_8 PIP_2, we quantified the EC_{50} of PIP_2 for activating desensitized TMEM16F channels. Following exposure of TMEM16F to 1 mM Ca^{2+}, we applied di-C_8 PIP_2. Restoration of TMEM16F activity was barely detectable at 1 μM di-C_8 PIP_2 and approached saturation at 20 μM di-C_8 PIP_2 (EC_{50} = 5.8 ± 0.5 μM, H = 2.2 ± 0.1) (Fig. 3 *E* and *F*).

The fact that PIP_2 depletion results in TMEM16F desensitization raises the question whether the active TMEM16F is associated with PIP_2. If channel association with PIP_2 is fully saturated, it should not be possible to further increase the background TMEM16F current by applying PIP_2. To test this possibility, we compared the effect of PIP_2 on Ca^{2+} sensitivity before and after desensitization and normalized the Ca^{2+} responses to the original maximal amplitude for each cell. Before desensitization of TMEM16F, di-C_8 PIP_2 did not increase the current magnitude, nor did it shift the Ca^{2+}-response curve. After desensitization, di-C_8 PIP_2 significantly increased the current magnitude and caused a left-shift of the Ca^{2+}-response curve (Fig. 3 *C* and *D*). Although the extent of current restoration at 10 μM PIP_2 was close to saturation (Fig. 3*F*), this current was still smaller than the current before desensitization, probably because di-C_8 PIP_2 could not be stably incorporated into the cell membrane for efficient stabilization of the open channel. These results support the view that TMEM16F constitutively binds PIP_2.

We then tested the specificity of PIP_2 binding by applying different PI derivatives. In addition to PIP_2, namely PI(4,5)P_2, we chose to test PI and some representative phosphoinositides

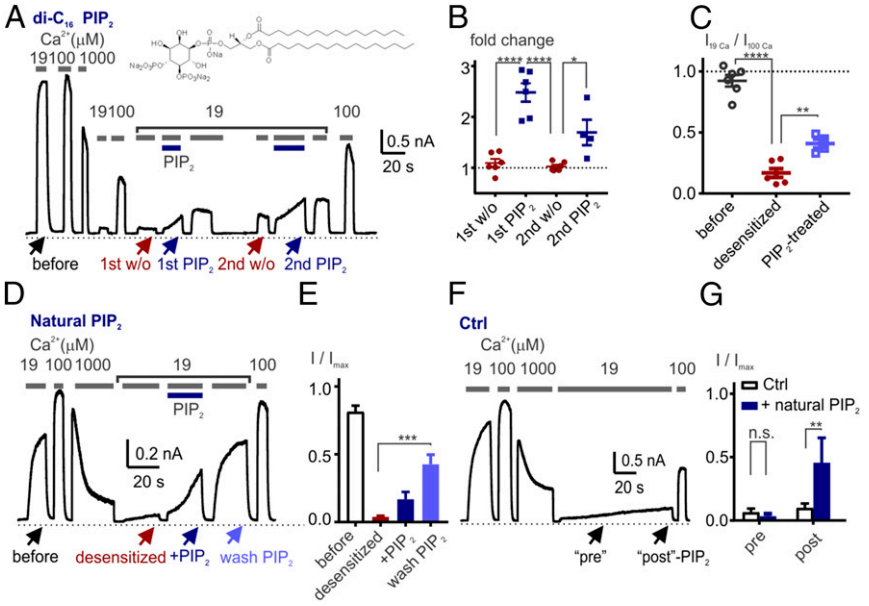

Fig. 2. Restoration from TMEM16F desensitization by application of exogenous PIP_2. (*A*) Representative recording showing di-C_{16} PIP_2-mediated restoration of TMEM16F current. After current inactivation, 19 μM Ca^{2+} with and without di-C_{16} PIP_2 (10 μM) were perfused repeatedly. Pairs of perfusion with 19 μM Ca^{2+} and 100 μM Ca^{2+} were applied at multiple points to estimate the extent of desensitization. (*B*) Scatter plots showing fold changes of current magnitude during application of 19 μM Ca^{2+} + di-C_{16} PIP_2 or 19 μM Ca^{2+} alone for 20 s. $^*P < 0.05$, $^{****}P < 0.0001$ (Tukey post hoc tests following one-way ANOVA). (*C*) Scatter plots showing the current magnitudes in 19 μM Ca^{2+} normalized by those in 100 μM Ca^{2+} within each pair of successive perfusions. $^{**}P < 0.01$, $^{****}P < 0.0001$ (Tukey post hoc tests following one-way ANOVA). (*D*) Representative recording showing restoration from TMEM16F desensitization by application of 20 μM natural purified PIP_2. (*E*) Summary of current magnitudes (in 19 μM Ca^{2+}) normalized by the current magnitudes during subsequent perfusions with 100 μM Ca^{2+} at time points indicated by arrows. $^{***}P < 0.001$ among indicated groups (one-way ANOVA); $n = 6$. (*F*) A representative recording in a control group that exhibited little recovery from desensitization. (*G*) Comparison of normalized current magnitudes at time points indicated by arrows between PIP_2-treated and control groups. $^{**}P < 0.01$, n.s. $P > 0.05$ (Sidak multiple comparison tests following two-way ANOVA); $n = 5$–6.

including PI(4)P, $PI(3,4)P_2$, $PI(3,5)P_2$, and $PI(3,4,5)P_3$. Notwithstanding variations across individual cells, phosphoinositides with more phosphates tend to be more efficient in restoring the desensitized TMEM16F current, and the minimal number of phosphates required is two (Fig. 3 *G* and *H*). We found that inositol-(1, 4, 5)-trisphosphate (IP_3) had no effect on desensitized

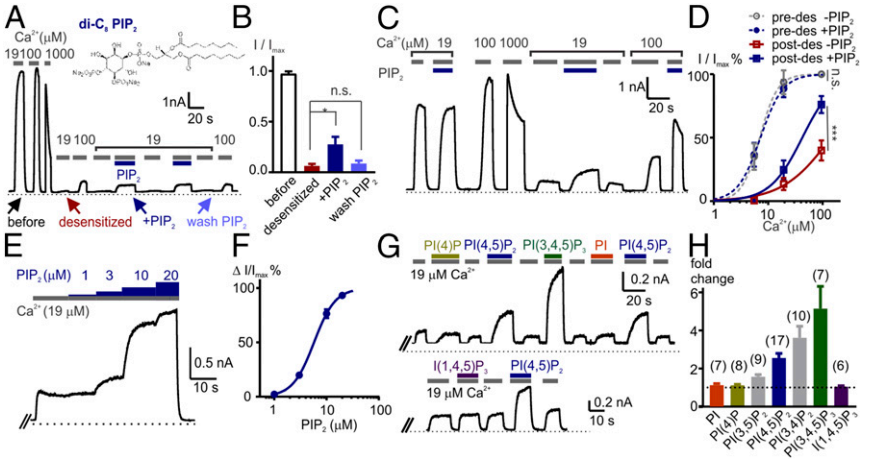

Fig. 3. Biophysical characterization of PIP_2 interaction with TMEM16F. (*A*) Representative recording showing reversible restoration from TMEM16F desensitization by application of di-C_8 PIP_2 (10 μM). (*B*) Summary of current magnitudes (in 19 μM Ca^{2+}) at time points indicated by arrows in *A* normalized by current magnitudes in 100 μM Ca^{2+}. One-way ANOVA revealed significant differences among currents in 19 μM Ca^{2+} with different treatments after patch exposure to 1 mM Ca^{2+} ($P < 0.05$), but the subsequent Tukey's multiple comparison indicated the difference between desensitized and wash PIP_2 did not reach significance. $P = 0.07$; $n = 6$. (*C*) Representative recording showing di-C_8 PIP_2 (10 μM) did not alter TMEM16F current before desensitization but enhanced the TMEM16F current after desensitization induced by exposure to 1 mM Ca^{2+}. (*D*) Ca^{2+} sensitivity of TMEM16F under indicated conditions. Current magnitudes under different conditions were each normalized to the current magnitude in 100 μM Ca^{2+} before desensitization and were fit with the Hill equation. n.s. $P > 0.05$, $^{***}P < 0.001$ (two-way ANOVA); $n = 3$–5. (*E*) Representative trace showing restoration from TMEM16F desensitization, which was induced by exposure to 1 mM Ca^{2+}, by di-C_8 PIP_2 in a dose-dependent manner. (*F*) Dose-dependence of di-C_8 PIP_2 for restoration of TMEM16F current following desensitization. Normalized currents were fit with the Hill equation; $n = 4$. (*G*) Representative recording showing the effects of 10 μM PI derivatives (all di-C_8 PIP_x) and $I(1,4,5)P_3$ on TMEM16F current following desensitization induced by exposure to 1 mM Ca^{2+}. (*H*) Summary of fold changes of current magnitudes induced by PI derivatives. $P < 0.0001$ (one-way ANOVA); $n = 6$–17 as indicated above each bar.

TMEM16F, suggesting that the diacylglycerol backbone is also necessary for PIP_2 interaction with TMEM16F (Fig. 3 *G* and *H*).

Positively Charged Amino Acids in the N-Terminal Domain Are Necessary for TMEM16F Interaction with PIP_2. Two possible scenarios have been proposed for protein interaction with PIP_2 (20, 22). One scenario, characteristic of PIP_2 interaction with the pleckstrin homology domain (PH domain) in DAPP1 (dual adaptor for phosphotyrosine and 3-phosphoinositides 1), involves multiple basic amino acids that are not adjacent to one another in the amino acid sequence but are in close proximity in the folded protein for specific interaction with PIP_2. Alternatively, a cluster of adjacent basic amino acids in the amino acid sequence may electrostatically interact with phosphoinositides and exhibit low selectivity among isomers, as is the case with the basic effector domain (BED) in MARCKS (myristoylated alanine-rich C kinase substrate). These two scenarios in many cases are not necessarily mutually exclusive (20, 22).

The observation that TMEM16F interacts with phosphoinositides with low specificity (Fig. 3 *G* and *H*) indicates that the structural basis of this PIP_2 interaction likely resembles that for the BED. We therefore searched for putative PIP_2-binding sites in the TMEM16F cytoplasmic regions that contain at least two consecutive positively charged residues. We neutralized these arginine and lysine residues and assessed the likelihood that they contribute to the PIP_2-binding sites based on the following three criteria: (*i*) mutants with complete deficiency of PIP_2 interaction would remain desensitized, so their Ca^{2+} sensitivity would be comparable to that of the desensitized wild-type channel; (*ii*) the Ca^{2+} sensitivity of the mutant channels would not be altered by exposure to 1 mM intracellular Ca^{2+}; and (*iii*) mutants unable to interact with PIP_2 would not respond to PIP_2 or $PI(3,4,5)P_3$ applied after the exposure to 1 mM Ca^{2+}. To take into account the possible redundancy of PIP_2-binding sites and the likely scenario that mutation of two basic amino acids might only partially reduce the PIP_2 affinity, we included all mutants with partial reduction of Ca^{2+} sensitivity in our study.

We found that a region rich in positively charged residues in the N-terminal domain of TMEM16F is involved in the interaction with PIP_2. Of the mutants tested for Ca^{2+} sensitivity, K87N_K88Q, R96S_K97Q, and K97N_R98Q had significantly reduced Ca^{2+} sensitivity (Fig. 4 *A* and *B* and Fig. S3*A*); after desensitization, their Ca^{2+} sensitivity was comparable to that of the desensitized wild-type channel (Fig. S3 *A* and *C*). It thus appears that the reduced Ca^{2+} sensitivity was caused by alterations to PIP_2 interaction. We further neutralized all six amino acids (K87N_K88Q_K95N_R96A_K97N_R98Q) and named this mutant "KKKRKR_NQNANQ." Its Ca^{2+} sensitivity closely mimicked that of desensitized wild-type TMEM16F and could not be further shifted by exposure to 1 mM Ca^{2+} (Fig. 4 *D*–*F*). In addition, di-C_8 PIP_2 or di-C_8 $PI(3,4,5)P_3$ failed to alter the magnitude of the current of this mutant in the presence of 19 μM Ca^{2+}, in contrast to their ability to restore activity of desensitized wild-type TMEM16F (Fig. 4 *C*, *D*, and *G*). We therefore concluded that this cluster of positively charged residues contributes to TMEM16F interaction with PIP_2. It remains possible that other amino acid residues may also contribute to PIP_2 coordination.

Synergy Between PIP_2 and Membrane Depolarization in Regulating TMEM16F Ca^{2+} Sensitivity. We wondered how the Ca^{2+} sensitivity of TMEM16F was modulated by PIP_2. As reported, the Ca^{2+} sensitivity of the TMEM16A Ca^{2+}-activated Cl^- channel is voltage-dependent. Depolarized membrane potential assists and stabilizes the binding of Ca^{2+} to the channel and thus increases Ca^{2+} sensitivity (28). The TMEM16F current is outwardly rectifying, so it is difficult to measure inward current at hyperpolarized membrane potential. We thus compared the Ca^{2+} sensitivity at +40 mV and +100 mV. TMEM16F at +100 mV was

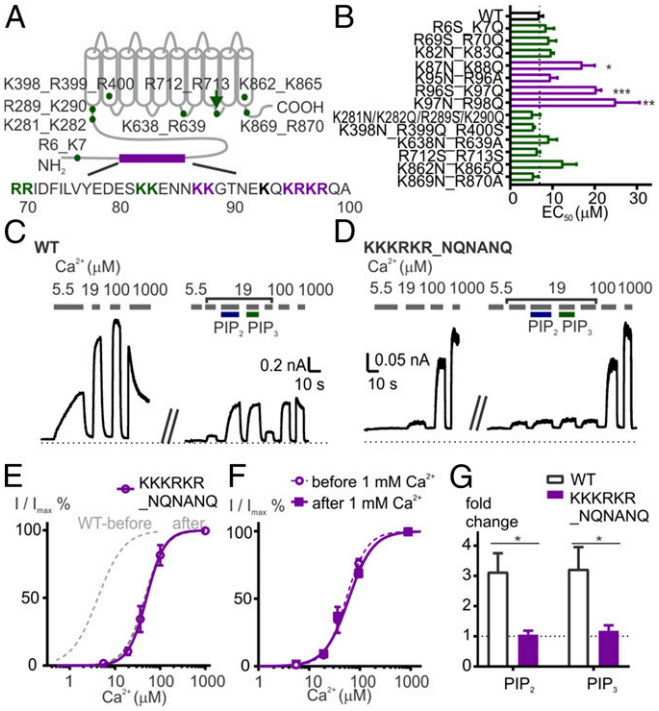

Fig. 4. Positively charged residues in the N-terminal domain are necessary for TMEM16F interaction with PIP_2. (*A*) A schematic of TMEM16F harboring consecutive basic residues in cytoplasmic domains. (*B*) The EC_{50}s of the Ca^{2+} responses of wild type and mutants. $*P < 0.05$, $**P < 0.01$, $***P < 0.001$, nonlabeled $P > 0.05$ (Dunn's tests following one-way Kruskal–Wallis test); $n = 3$–7. (*C* and *D*) Representative recordings of wild-type TMEM16F (*C*) and the KKKRKR_NQNANQ mutant (*D*) exposed to four different concentrations of Ca^{2+}. Exposure to 1 mM Ca^{2+} was followed with application of 10 μM di-C_8 PIP_2 and di-C_8 $PI(3,4,5)P_3$ in 19 μM Ca^{2+}. (*E*) Comparison of Ca^{2+} sensitivity of the KKKRKR_NQNANQ mutant with wide-type TMEM16F. The Kruskal–Wallis test suggested there were significant differences in EC_{50} among the three groups ($P < 0.0001$). The subsequent Dunn's multiple comparison indicated the EC_{50} of KKKRKR_NQNANQ was significantly different from wild type before desensitization ($P < 0.01$, $n \geq 5$) but not after desensitization ($P = 0.8$, $n \geq 5$). (*F*) Ca^{2+} sensitivity of KKKRKR_NQNANQ before and after exposure to 1 mM Ca^{2+}. $P = 0.13$ in EC_{50} between the two groups (Wilcoxon matched-pairs test); $n = 5$. (*G*) Summary of fold changes of currents treated with 10 μM di-C_8 PIP_2 or di-C_8 PIP_3. $*P < 0.05$ (Sidak multiple comparison tests following two-way ANOVA); $n \geq 6$.

significantly more sensitive to Ca^{2+} compared with TMEM16F at +40 mV (at +100 mV, $EC_{50} = 4.8 \pm 0.6$ μM, $H = 2.1 \pm 0.3$; at +40 mV, $EC_{50} = 9.5 \pm 0.5$ μM, $H = 2.1 \pm 0.2$; $n = 5$) (Fig. 5 *A* and *B*). Thus, similar to its nonscrambling paralog TMEM16A, TMEM16F also displays voltage-dependent Ca^{2+} sensitivity.

If depolarization and TMEM16F interaction with PIP_2 have synergistic effects on Ca^{2+} sensitivity, depletion of PIP_2 is expected to not only reduce Ca^{2+} sensitivity but also change the voltage-dependence of activation, so that the channel requires greater depolarization to open. Indeed, compared with currents at 4 μM Ca^{2+}, currents at 15 μM Ca^{2+} could be activated at a lower voltage, so that the normalized G–V curve for the conductance (G)–voltage (V) relationship was left-shifted (Fig. 5*D*). PIP_2 depletion following prolonged exposure of the patch to 1 mM Ca^{2+} caused a right shift of the G–V relationship (Fig. 5 *C* and *E*), so that a stronger depolarization is required to open the channel. The G–V relationship of the PIP_2-irresponsive mutant KKKRKR_NQNANQ closely resembles that of the wild-type channel after exposure to 1 mM Ca^{2+} (Fig. 5 *C* and *E*). In 1 mM Ca^{2+}, which causes PIP_2 to be hydrolyzed by phospholipases, wild-type and mutant channels displayed similar voltage-dependence

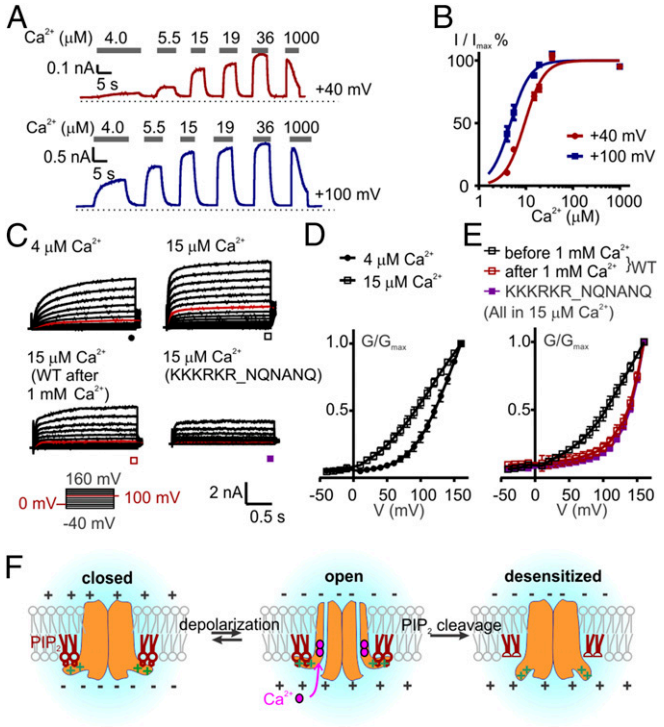

Fig. 5. PIP_2 acts synergistically with membrane depolarization to regulate Ca^{2+} sensitivity. (*A*) Representative recordings of TMEM16F current at +40 mV (*Upper*) and at +100 mV (*Lower*). (*B*) Ca^{2+} sensitivity of TMEM16F at +40 mV and +100 mV. $P < 0.01$ for the difference of EC_{50} between the two groups (two-tailed Mann–Whitney test); $n = 5$. (*C*) Representative voltage-clamp recordings of TMEM16F currents under the indicated conditions. The currents were recorded from inside-out patches. The patches were held at 0 mV and subjected to pulses from −40 mV to +160 mV with 10-mV increments. The current recorded at +100 mV is shown in red for comparison. (*D*) Normalized G–V relationships of wild-type TMEM16F current in 15 μM Ca^{2+} and 4 μM Ca^{2+}. $P < 0.001$ between the two conditions (two-way ANOVA); $n = 4$. (*E*) G–V relationships of wild-type TMEM16F before and after exposure to 1 mM Ca^{2+} and KKKRKR_NQNANQ without exposure to 1 mM Ca^{2+} ($n \geq 4$). Two-way ANOVA suggested there was a significant difference in normalized current amplitudes for wild type before and after 1 mM Ca^{2+} ($P < 0.01$), but the current of wild-type channels after exposure to 1 mM Ca^{2+} was not significantly different from the current of the KKKRKR_NQNANQ mutant ($P = 0.48$). (*F*) A proposed model for synergistic regulation by PIP_2 and membrane depolarization of Ca^{2+}-gating of TMEM16F.

(Fig. S4 *B* and *C*). These results support a synergy between PIP_2 and depolarization in their regulation of Ca^{2+}-gating of TMEM16F.

The schematic shown in Fig. 5*F* illustrates the hypothetical mechanism of PIP_2 regulation of the Ca^{2+}-activated TMEM16F channel. PIP_2 is located at the inner leaflet of the lipid bilayer and electrostatically interacts with the positive charges at the N-terminal cytoplasmic domain of TMEM16F. TMEM16F–PIP_2 interaction may facilitate or stabilize the TMEM16F conformational change induced by membrane depolarization that drives Ca^{2+} ions into the transmembrane domain harboring the Ca^{2+}-binding sites to open the channel (Fig. 5*F*). Hydrolysis of PIP_2 by Ca^{2+}-dependent phospholipase (27, 29) or other signaling pathways (19), reduces the ability of both Ca^{2+} and membrane depolarization to activate the channel, thus providing a brake to terminate TMEM16F activities and prevent excessive permeation of cations including Ca^{2+}.

Discussion

TMEM16F-mediated phospholipid scrambling closely correlates with TMEM16F ion conductivity (17), allowing us to probe the functions of TMEM16F from the ion-channel perspective. In this study, we examined the dependence of TMEM16F function on PIP_2. Depletion of PIP_2 triggers channel rundown as well as desensitization, which can be reversed by the application of exogenous PIP_2. Our results indicate that PIP_2 binds to a cluster of positively charged amino acids near the N terminus via electrostatic interactions, thereby regulating Ca^{2+}-gating of TMEM16F in a way synergistic with channel modulation by membrane depolarization.

Structural Basis for PIP_2 Interaction. Diversity of PIP_2-binding sites in various proteins notwithstanding, clusters of positively charged amino acids are the common features. Two models have been proposed to describe the structural bases for protein interaction with PIP_2, although proteins may employ both strategies (20, 22). In PH domains, the basic amino acids that interact with PIP_2 are not adjacent to one another in the amino acid sequence, but in folded proteins they are spatially close to coordinate PIP_2. These binding sites are usually specific to PIP_2, while other phosphoinositide isomers exhibit little or no binding. In contrast, the BED in MARCKS represents another structural basis for a PIP_2-binding site, where more than 10 basic amino acids are clustered in the primary amino acid sequence and generate a strong electrostatic field for nonspecific interactions with negatively charged head groups of phosphoinositides. As for TMEM16F, restoration of channel activity by $PI(3,4)P_2$, $PI(3,5)P_2$, and $PI(3,4,5)P_3$ (Fig. 3 *G* and *H*) indicates that the structural basis for PIP_2 binding might arise from electrostatic and nonspecific interactions with negatively charged phosphoinositides. Our finding that a cluster of basic amino acids at the N terminus is necessary for PIP_2 interaction is consistent with this scenario.

Although the charges of K87, K88, K95, R96, K97, and R98 appear necessary to coordinate PIP_2, they might not be sufficient for the interaction. The Kir2.2 coordination with PIP_2 in structural studies suggests that some of its basic amino acids (R65, R190, and R219) strengthen the interaction between Kir2.2 and PIP_2 (22, 30). Although we did not identify other double mutants with severe PIP_2-binding defects, we cannot rule out the potential participation of other residues with allosteric effects on PIP_2 coordination. In addition, Kir channels also have a conserved RWR sequence in the transmembrane domains that interacts with the 1′ phosphate, glycerol backbone, and acyl chains (30). Our finding that IP_3 cannot rescue the desensitization suggests that the diacylglycerol backbone is also necessary to trigger the restoration of TMEM16F channel activity, but the structural basis is yet to be identified.

The cluster of basic amino acids at the N terminus is not conserved in other TMEM16 family members, which are localized in different parts of the cells (10, 14, 31). The structural basis for PIP_2 regulation might reflect the adaptation of TMEM16F to its functions at the cell membrane. Some of the TMEM16 proteins that are localized to the cell membrane, such as the TMEM16A calcium-activated chloride channel, have several dispersed basic amino acids at similar positions, suggesting that the potential phosphoinositide regulation may involve mechanisms potentially different from that for TMEM16F. Interestingly, the fungal homologs with scramblase activity, nhTMEM16 and afTMEM16 (15, 32), do not have the conserved cluster of positive charges at the N terminus, likely reflecting the divergence of membrane lipid signaling between fungi and animals.

Gating of TMEM16F. Intracellular calcium activates the TMEM16A and TMEM16B calcium-activated chloride channels in a voltage-dependent manner, with higher Ca^{2+} sensitivity at more depolarized membrane potentials (11, 33, 34). This voltage dependence of Ca^{2+} sensitivity could arise from the ability of membrane depolarization to drive Ca^{2+} ions into the membrane electric field to reach their binding sites (28). As a hallmark feature of these calcium-activated chloride channels, TMEM16A displays outward

rectification at low Ca^{2+} but shows no voltage dependence at high Ca^{2+}. In central neurons, the voltage-dependence of calcium-activated chloride channels allows the channels to conduct anions upon depolarization to prevent overexcitation at low intracellular Ca^{2+} and to remain open at all voltages to keep the cells quiescent at high intracellular Ca^{2+}.

TMEM16F differs from TMEM16A and TMEM16B in that it is permeable to cations, including Ca^{2+} (6). If TMEM16F is constantly open at high Ca^{2+}, Ca^{2+}-influx through TMEM16F channels will constitute positive feedback and lead to cell death. To prevent this detrimental outcome, TMEM16F may utilize PIP_2 as a sensor for intracellular Ca^{2+}. At low Ca^{2+}, membrane depolarization and PIP_2 work synergistically to assist or stabilize Ca^{2+} binding and channel activation, so that the channel can open to amplify the excitation. The hydrolysis of PIP_2 by phospholipase that is activated at high cytosolic Ca^{2+} causes TMEM16F to require a much stronger depolarization, which cannot be readily achieved, for its sustained activity. Thus, PIP_2 may work as an allosteric regulator for TMEM16F, and its hydrolysis can presumably terminate TMEM16F-mediated signaling.

Physiological Significance of TMEM16F–PIP_2 Interaction. The dependence of TMEM16F activity on PIP_2 suggests that during protein synthesis and trafficking TMEM16F is mostly confined in a desensitized conformation. PIP_2 is a minor but specific constituent of the cell membrane, while the major components of PI derivatives in the endoplasmic reticulum and Golgi apparatus are nonphosphorylated PI and monophosphorylated PI(4)P (1, 23), respectively, neither of which can support TMEM16F activity (Fig. 3 *G* and *H*). Thus, even with elevated intracellular Ca^{2+}, TMEM16F is expected to be barely active in intracellular organellar membranes. Although the lysosome is abundant in PI $(3,5)P_2$, its function in protein degradation and its unique compartmental environment may not be compatible with TMEM16F function, and TMEM16F localization in lysosomes has not been reported thus far. Thus, PIP_2 may serve as a permissive signaling molecule for TMEM16F activity on the cell membrane.

PIP_2 is also a potential modulator for TMEM16F functions in physiological processes. TMEM16F gating regulation by PIP_2 may function as a terminator that breaks the positive feedback loop to prevent excessive Ca^{2+} influx. In some signaling pathways involving G_q-protein activation, phospholipase C cleaves PIP_2 into IP_3 and diacylglycerol (19). Desensitization caused by PIP_2 cleavage might reduce TMEM16F activity during sustained Ca^{2+} elevation resulting from IP_3-induced Ca^{2+}-release from the endoplasmic reticulum. It is also worth noting that $PI(3,4,5)P_3$ potentiates TMEM16F with slightly greater efficacy than PIP_2 (Fig. 3 *G* and *H*). $PI(3,4,5)P_3$ has restricted distribution on specialized patches of the cell membrane, such as the leading edges of neutrophils during chemotaxis and migration (35). It would be of interest to test whether sensitization of TMEM16F by $PI(3,4,5)P_3$ contributes to membrane reshaping at the leading edges of migrating cells.

TMEM16F-mediated lipid scrambling exposes phosphatidylserine to the platelet surface, which provides the platform for the assembly of blood coagulation factors (5, 6). Since TMEM16F ion channel activities correlate with its scramblase functions (17), PIP_2 metabolic pathways could potentially be pharmaceutical targets for diseases associated with pathological blood clotting such as thrombosis. Given the broad distribution of TMEM16F in a variety of tissues (36) with its roles yet to be identified, it will be of interest to explore the physiological implications of phosphoinositide regulation of TMEM16F in different cell types.

Materials and Methods

Cell Culture and Molecular Biology. Mouse *Tmem16f* cDNA [sequence as in National Center for Biotechnology Information (NCBI) RefSeq NM_175344.4] was generated as previously reported (6) and subcloned into pmCherry-N1 vector via standard molecular biology techniques. Site-directed mutagenesis was performed using Phusion polymerase (New England Biolabs), and all sequences were verified (Quintara Biosciences). HEK293 cells were cultured in DMEM with 4.5 g/L glucose, L-glutamine, and sodium pyruvate (Mediatech) containing 10% FBS (Axenia BioLogix) and 1% penicillin-streptomycin, at 37 °C and with 5% CO_2. Cells were lifted with trypsin-EDTA (Life Technologies) and plated onto 12 mm coverslips (Warner Instruments) 3–4 d before recording. Transient transfection was performed with Lipofectamine 2000 (Thermo Fisher Scientific) 2 d before recording. The cDNA constructs for wild-type TMEM16F-mCherry and the mutant KKKRKR_NQNANQ-mCherry were also subcloned into pENTR1A (Addgene plasmid no. 17398) and transferred to pLenti CMV Hygro DEST (Addgene plasmid no. 17454) using Gateway cloning (37). pENTR1A no ccDB (w48-1) and pLenti CMV Hygro DEST (w117-1) were gifts from Eric Campeau and Paul Kaufman, University of Massachusetts Medical School, Worcester, MA. TMEM16F-mCherry pLenti was cotransfected into HEK293FT cells with packaging plasmids pMD.2G and psPAX2 (Addgene plasmids no. 12259 and no. 12260), which were gifts from Didier Trono, École Polytechnique Fédérale de Lausanne, Lausanne, Switzerland. Lentivirus was harvested from the transfected cells 36–48 h posttransfection and incubated with HEK293 cells to establish stable cell lines under hygromycin selection. Data in Figs. 1–3 and 5 and Figs. S1, S2, and S4 are recordings from stable cell lines.

Solutions. For electrophysiology recordings, bath solution contained 145 mM NaCl, 10 mM Hepes, 2 mM $CaCl_2$, 1 mM $MgCl_2$, 10 mM glucose (pH 7.2) with NaOH. Pipette solution contained 150 mM NaCl, 10 mM Hepes, 1 mM $CaCl_2$, unless otherwise stated. The membrane patch was excised to form the inside-out configuration in Ca^{2+}-free solution: 150 mM NaCl, 10 mM Hepes, 2 mM EGTA. For solutions with Ca^{2+} <100 μM, Ca^{2+} was added to solutions containing 2 mM EGTA or 2 mM HEDTA [*N*-(hydroxyethyl)-ethylenediaminetriacetic acid], and the final concentration was confirmed with Oregon Green BAPTA 5N (Thermo Fisher Scientific). The osmolality of each solution was adjusted to 290–310 mOsm/kg. di-C_{16} PIP_2, di-C_8 PIP_2, and all the chemicals used in the experiments shown in Fig. 3 *G* and *H* were purchased from Echelon Biosciences. Natural PIP_2 was purchased from Avanti Polar Lipids. All other chemicals were purchased from Sigma-Aldrich.

Electrophysiology. Coverslips with cells were transferred to a recording chamber on a Nikon-TE2000 Inverted Scope (Nikon Instruments), and transfection was confirmed with fluorescent microscopy. Patch borosilicate pipets (Sutter Instrument) were pulled from a Sutter P-97 puller with resistances of 2–3 MΩ for inside-out patch recordings. Solutions were puffed to the excised patch using VC3-8xP pressurized perfusion system (ALA Science). Data were acquired using a Multiclamp 700B amplifier controlled by Clampex 10.2 via Digidata 1440A (Axon Instruments). All experiments were performed at room temperature (22–24 °C).

Data Analysis. All data were analyzed using pClamp10 (Molecular Devices), OriginLab (OriginLab Corporation), and GraphPad Prism (GraphPad Software). For the measurement of Ca^{2+} sensitivity, every trace was fit with the Hill equation to generate its respective EC_{50} and H. The curves in the figures display the averaged current magnitudes normalized to their respective maximal values (I/I_{max} %). Significant differences were determined with indicated nonparametric comparisons for the EC_{50}s of Ca^{2+}-response curves or with Student's *t* test and ANOVA for other values unless otherwise stated. In all cases except Fig. S2*B*, data represent mean ± SEM; $*P < 0.05$, $**P < 0.01$, $***P < 0.001$, $****P < 0.0001$, n.s. $P > 0.05$.

ACKNOWLEDGMENTS. We thank Dr. Michael Grabe, Neville Bethel, Dr. Christian Peters, Dr. Mu He, Dr. Shengjie Feng, and Dr. Maja Petkovic (University of California, San Francisco) for helpful discussions. Y.N.J. and L.Y.J. are investigators of the Howard Hughes Medical Institute. This study is supported by the NIH Grant NS069229 (to L.Y.J.).

1. van Meer G, Voelker DR, Feigenson GW (2008) Membrane lipids: Where they are and how they behave. *Nat Rev Mol Cell Biol* 9:112–124.
2. Nagata S, Suzuki J, Segawa K, Fujii T (2016) Exposure of phosphatidylserine on the cell surface. *Cell Death Differ* 23:952–961.
3. Segawa K, Nagata S (2015) An apoptotic 'Eat Me' signal: Phosphatidylserine exposure. *Trends Cell Biol* 25:639–650.
4. Bevers EM, Williamson PL (2016) Getting to the outer leaflet: Physiology of phosphatidylserine exposure at the plasma membrane. *Physiol Rev* 96:605–645.

5. Suzuki J, Umeda M, Sims PJ, Nagata S (2010) Calcium-dependent phospholipid scrambling by TMEM16F. *Nature* 468:834–838.
6. Yang H, et al. (2012) TMEM16F forms a Ca^{2+}-activated cation channel required for lipid scrambling in platelets during blood coagulation. *Cell* 151:111–122.
7. Castoldi E, Collins PW, Williamson PL, Bevers EM (2011) Compound heterozygosity for 2 novel *TMEM16F* mutations in a patient with Scott syndrome. *Blood* 117: 4399–4400.
8. Whitlock JM, Hartzell HC (2017) Anoctamins/TMEM16 proteins: Chloride channels flirting with lipids and extracellular vesicles. *Annu Rev Physiol* 79:119–143.
9. Picollo A, Malvezzi M, Accardi A (2015) TMEM16 proteins: Unknown structure and confusing functions. *J Mol Biol* 427:94–105.
10. Pedemonte N, Galietta LJ (2014) Structure and function of TMEM16 proteins (anoctamins). *Physiol Rev* 94:419–459.
11. Schroeder BC, Cheng T, Jan YN, Jan LY (2008) Expression cloning of TMEM16A as a calcium-activated chloride channel subunit. *Cell* 134:1019–1029.
12. Caputo A, et al. (2008) TMEM16A, a membrane protein associated with calcium-dependent chloride channel activity. *Science* 322:590–594.
13. Yang YD, et al. (2008) TMEM16A confers receptor-activated calcium-dependent chloride conductance. *Nature* 455:1210–1215.
14. Suzuki J, et al. (2013) Calcium-dependent phospholipid scramblase activity of TMEM16 protein family members. *J Biol Chem* 288:13305–13316.
15. Brunner JD, Lim NK, Schenck S, Duerst A, Dutzler R (2014) X-ray structure of a calcium-activated TMEM16 lipid scramblase. *Nature* 516:207–212.
16. Paulino C, et al. (2017) Structural basis for anion conduction in the calcium-activated chloride channel TMEM16A. *Elife* 6:26232.
17. Yu K, et al. (2015) Identification of a lipid scrambling domain in ANO6/TMEM16F. *Elife* 4:e06901.
18. Scudieri P, et al. (2015) Ion channel and lipid scramblase activity associated with expression of TMEM16F/ANO6 isoforms. *J Physiol* 593:3829–3848.
19. Balla T (2013) Phosphoinositides: Tiny lipids with giant impact on cell regulation. *Physiol Rev* 93:1019–1137.
20. Suh BC, Hille B (2008) PIP_2 is a necessary cofactor for ion channel function: How and why? *Annu Rev Biophys* 37:175–195.
21. Logothetis DE, et al. (2015) Phosphoinositide control of membrane protein function: A frontier led by studies on ion channels. *Annu Rev Physiol* 77:81–104.
22. Hansen SB (2015) Lipid agonism: The PIP_2 paradigm of ligand-gated ion channels. *Biochim Biophys Acta* 1851:620–628.
23. Hille B, Dickson EJ, Kruse M, Vivas O, Suh BC (2015) Phosphoinositides regulate ion channels. *Biochim Biophys Acta* 1851:844–856.
24. Gamper N, Rohacs T (2012) Phosphoinositide sensitivity of ion channels, a functional perspective. *Subcell Biochem* 59:289–333.
25. Gamper N, Shapiro MS (2007) Regulation of ion transport proteins by membrane phosphoinositides. *Nat Rev Neurosci* 8:921–934.
26. Várnai P, Balla T (1998) Visualization of phosphoinositides that bind pleckstrin homology domains: Calcium- and agonist-induced dynamic changes and relationship to myo-[^{3}H]inositol-labeled phosphoinositide pools. *J Cell Biol* 143:501–510.
27. Rhee SG (2001) Regulation of phosphoinositide-specific phospholipase C. *Annu Rev Biochem* 70:281–312.
28. Dang S, et al. (2017) Cryo-EM structures of the TMEM16A calcium-activated chloride channel. *Nature* 552:426–429.
29. Horowitz LF, et al. (2005) Phospholipase C in living cells: Activation, inhibition, Ca^{2+} requirement, and regulation of M current. *J Gen Physiol* 126:243–262.
30. Hansen SB, Tao X, MacKinnon R (2011) Structural basis of PIP_2 activation of the classical inward rectifier K^+ channel Kir2.2. *Nature* 477:495–498.
31. Duran C, Qu Z, Osunkoya AO, Cui Y, Hartzell HC (2012) ANOs 3-7 in the anoctamin/Tmem16 Cl^- channel family are intracellular proteins. *Am J Physiol Cell Physiol* 302: C482–C493.
32. Malvezzi M, et al. (2013) Ca^{2+}-dependent phospholipid scrambling by a reconstituted TMEM16 ion channel. *Nat Commun* 4:2367.
33. Tien J, et al. (2014) A comprehensive search for calcium binding sites critical for TMEM16A calcium-activated chloride channel activity. *Elife* 3:2772.
34. Cenedese V, et al. (2012) The voltage dependence of the TMEM16B/anoctamin2 calcium-activated chloride channel is modified by mutations in the first putative intracellular loop. *J Gen Physiol* 139:285–294.
35. Franca-Koh J, Kamimura Y, Devreotes PN (2007) Leading-edge research: PtdIns(3,4,5)P_3 and directed migration. *Nat Cell Biol* 9:15–17.
36. Gritli-Linde A, et al. (2009) Expression patterns of the *Tmem16* gene family during cephalic development in the mouse. *Gene Expr Patterns* 9:178–191.
37. Campeau E, et al. (2009) A versatile viral system for expression and depletion of proteins in mammalian cells. *PLoS One* 4:e6529.